CMS Physics Analysis Summary

Contact: cms-pag-conveners-exotica@cern.ch 2018/07/06

Search for excited leptons in the $\ell\ell\gamma$ final state in proton-proton collisions at $\sqrt{s} = 13$ TeV

The CMS Collaboration

Abstract

A search is presented for excited electrons and muons using a data sample of proton-proton collisions at a center-of-mass energy of $\sqrt{s} = 13$ TeV, collected with the CMS detector in 2016 and corresponding to an integrated luminosity of 35.9 fb^{-1}. This is the first search in the $\ell\ell\gamma$ final state in proton-proton collisions at $\sqrt{s} = 13$ TeV. The observed data are consistent with the standard model prediction, and exclusion limits on the excited lepton mass and the compositeness scale are set. Excited electrons (muons) with a mass below 3.9 (3.8) TeV are excluded under the assumption that the excited lepton mass equals the compositeness scale. The best observed limit on the compositeness scale is obtained in the mass range between 0.5 and 1.0 TeV, excluding a compositeness scale below 25 TeV for both excited electrons and muons. These are the most stringent limits to date in the $\ell\ell\gamma$ final state.

1 Introduction

The standard model (SM) provides an extremely precise description of various phenomena in particle physics observed over the last half century. Notwithstanding its huge success, it does not adequately explain the origin of the mass hierarchy and the three generations of quarks and leptons. As an attempt to answer such fundamental questions, compositeness of quarks and leptons is introduced in many models [1–11]. These compositeness models suggest that quarks and leptons are the bound states of more fundamental constituents that are bound by a new strong interaction with a characteristic scale Λ (called the compositeness scale).

A prediction of compositeness models is the existence of excited states of quarks and leptons. In proton-proton collisions, excited fermions could be produced via contact interactions (CI) and decay either through SM gauge interactions or via CI to SM fermions.

This result presents a search for excited leptons (ℓ^*) in the $\ell\ell\gamma$ final state ($\ell\ell^* \to \ell\ell\gamma$), where the decay of the excited lepton is mediated by a photon, in the mass range $0.25 \leq M_{\ell^*} \leq 5\,\text{TeV}$. We consider a benchmark model based on the formalism described in Ref. [7].

Several searches for excited leptons have been previously performed by the CMS Collaboration [12, 13], but no evidence for excited leptons was found, excluding $M_{\ell^*} < 2.5\,\text{TeV}$ for the case $M_{\ell^*} = \Lambda$. Searches at the LEP [14–17], HERA [18], Tevatron [19–22] colliders, and by the ATLAS collaboration at the CERN LHC with proton-proton collision data collected at $\sqrt{s} = 7\,\text{TeV}$ [23] and $\sqrt{s} = 8\,\text{TeV}$ [24] also have not found any evidence for the existence of excited leptons, setting a lower mass limit of 2.2 TeV [24] for the case $M_{\ell^*} = \Lambda$.

2 The CMS detector

The central feature of the CMS apparatus is a superconducting solenoid of 6 m internal diameter, providing a magnetic field of 3.8 T. Within the solenoid volume are a silicon pixel and strip tracker, a lead tungstate crystal electromagnetic calorimeter (ECAL), and a brass and scintillator hadron calorimeter (HCAL), each composed of a barrel and two endcap sections. Forward calorimeters extend the pseudorapidity (η) coverage provided by the barrel and endcap detectors. Muons are detected in gas-ionization chambers embedded in the steel flux-return yoke outside the solenoid.

A more detailed description of the CMS detector, together with a definition of the coordinate system used and the relevant kinematic variables, can be found in Ref. [25].

Events of interest are selected using a two-tiered trigger system [26]. The first level, composed of custom hardware processors, uses information from the calorimeters and muon detectors to select events at a rate of less than 100 kHz within a time interval of less than 4 μs. The second level, known as the high-level trigger, consists of a farm of processors running a version of the full event reconstruction software optimized for fast processing, and reduces the event rate to around 1 kHz before data storage.

3 Data and simulated samples

The data used for this analysis correspond to an integrated luminosity of $35.9\,\text{fb}^{-1}$, recorded with the CMS detector in proton-proton collisions at a center-of-mass energy of 13 TeV in 2016. The data sample for the eeγ channel consists of events that are selected using double-electron triggers with a threshold on the transverse energy of the calorimeter cluster of 33 GeV for both

electron candidates. For the $\mu\mu\gamma$ channel, events are selected using single-muon triggers with a threshold of 24 GeV on the transverse momentum, p_T, of the muon.

Simulated signal events are generated for excited lepton masses ranging from 0.25 TeV to 5 TeV, using PYTHIA 8.205 [27]. The CUETP8M1 [28, 29] underlying-event tune is used for all simulated samples. The samples are generated at the compositeness scale $\Lambda = 10$ TeV, but are also used for different compositeness scale interpretations since the compositeness scale does not affect the kinematic distributions of final state particles. The simulated signals are generated at leading order (LO) in perturbative quantum chromodynamics (QCD) and a mass dependent k-factor for next-to-leading-order (NLO) corrections is applied [30].

Major SM backgrounds such as $Z\gamma$ and $t\bar{t}\gamma$ processes are generated at NLO using the MADGRAPH5_aMC@NLO 2.3.3 generator [31], while WW, WZ, and ZZ backgrounds are generated at LO with PYTHIA 8.205. The cross section for WW is calculated to next-to-next-to-leading order and the cross sections for WW and WZ are computed at NLO.

The effect of multiple proton-proton interactions within the same bunch crossing or adjacent bunch crossings (pileup) is taken into account for simulation and simulated events are weighted to match the observed pileup distribution in the data sample.

4 Event selection

The particle-flow algorithm [32] aims to reconstruct and identify individual particles in an event using an optimized combination of information from the various elements of the CMS detector. The energy of photons is directly obtained from the ECAL measurement, corrected for zero-suppression effects. The energy of electrons is determined from a combination of the electron momentum at the primary interaction vertex as determined by the tracker, the energy of the corresponding ECAL cluster, and the energy sum of all bremsstrahlung photons spatially compatible with originating from the electron track. The momentum of muons is obtained from the curvature of the corresponding track. The energy of charged hadrons is determined from a combination of their momentum measured in the tracker and the matching ECAL and HCAL energy deposits, corrected for zero-suppression effects and for the response function of the calorimeters to hadronic showers. Finally, the energy of neutral hadrons is obtained from the corresponding corrected ECAL and HCAL energies.

Events must have at least one primary vertex with at least four associated tracks, with the transverse (longitudinal) position within 2 (24) cm from the nominal collision point. The reconstructed vertex with the largest value of summed physics-object p_T^2 is taken to be the primary pp interaction vertex. The physics objects are the jets, clustered using a jet finding algorithm [33, 34] with the tracks assigned to the vertex as inputs, and the associated missing transverse momentum, taken as the negative vector sum of the p_T of those jets.

Electrons candidates are reconstructed from clusters of ECAL energy deposits associated with tracks reconstructed in the inner tracking systems. The electron candidates are required to have $p_T > 35$ GeV and to be within the region of $|\eta| < 2.5$. The barrel-endcap transition region $1.44 < |\eta| < 1.56$ is excluded because of the high rate of poorly reconstructed electrons. The electron candidates have to pass a set of identification requirements on the distribution of energy deposits in the ECAL, on the ratio of the associated HCAL and ECAL energy deposits, on the isolation in the calorimeters, on the quality of the matching between the ECAL clusters and the associated track in the inner tracker, and on the agreement between the energy reconstructed in the ECAL and the momentum of the associated track.

Muon candidates are reconstructed as tracks in the muon detector that are matched to the tracks found in the inner tracker. The muon candidates must have $p_T > 35\,\text{GeV}$ and be within $|\eta| < 2.4$. The muon candidates are required to pass identification criteria that are dedicated to muons having high transverse momentum [35] and to be isolated in the tracking systems.

Photons reconstruction starts from the energy deposits in the ECAL and reconstructed candidates that have associated tracks are rejected. The photon candidates are required to have $p_T > 35\,\text{GeV}$ and $|\eta| < 2.5$, with those in the transition region $1.44 < |\eta| < 1.56$ being excluded from the analysis. A multivariate analysis (MVA) technique is used for photon identification, with shower shape variables and photon isolation sums in the ECAL and HCAL as inputs [36, 37].

Events are required to have two same-flavor leptons and a photon. No condition is required on the charges of the leptons, to maximize the event selection efficiency. The selected leptons must be separated from the photon by $\Delta R = \sqrt{\Delta\eta^2 + \Delta\phi^2} > 0.7$. In addition, the invariant mass of the two same-flavor leptons is required to be larger than 116 GeV in order to suppress the dominant background contribution that comes from Z boson production.

5 Background modeling

The major backgrounds in this search originate from SM processes with final states consisting of two prompt same-flavor leptons and a prompt photon or a jet. The expected fraction of background events that have a jet misidentified as a lepton is less than 1% [38], therefore this background source is not considered in the analysis. Backgrounds associated with a prompt photon are estimated using simulation, while the yield of those associated with a jet is derived from the data.

The most dominant background arises from Z boson production accompanied by a prompt photon ($Z\gamma$), which has a signature similar to the signal. It is efficiently suppressed by applying Z-veto criteria described in Section 4. The fraction of $Z\gamma$ events after event selection and requiring the Z-veto criteria is approximately 70% of the total background.

Another prompt photon background comes from top pair production in association with a photon ($t\bar{t}\gamma$). These events form approximately 10% of the total background. In addition, there are backgrounds from triboson processes such as $WW\gamma$, $WZ\gamma$, and $ZZ\gamma$, whose contribution is small compared to other prompt photon backgrounds.

The other major background contribution consists of events with two prompt leptons and a jet misidentified as a photon, hereafter referred to as the jet background. The jet background estimation is derived from data events in a control region defined by photon candidates passing all kinematic selections but failing the photon selection. The control region events, scaled by the misidentification rate of photon candidates from jets, provide the jet background prediction in the signal region.

The misidentification rate is measured as a function of photon p_T and η by fitting template distributions of a MVA output variable for prompt photons and photons from jets to the data sampled by requiring two same-flavor leptons with an invariant mass between 50 and 116 GeV and one reconstructed photon candidate. A template distribution for prompt photons is obtained from simulated prompt photon background events passing the same selection as used for the data sample. The MVA variable distribution of W-tagged events in data is used for photons from the jets. The measured misidentification rate ranges from 2 (3)% at $p_T = 35\,\text{GeV}$ to 0.2 (0.4)% at 1 TeV in the detector barrel (endcaps). The estimated background events from jets

misidentified as a photon correspond to 5–15% of the events in the signal region.

After applying the measured misidentification rate, a further correction to the kinematic distribution of the estimated background is needed. The kinematic distributions of the parent jets of the misidentified photons in the control region and those of the signal region are not identical in the same photon p_{T} range, due to isolation requirements in the MVA identification. Consequently, the transverse momentum distributions of leptons, which are correlated with the recoil of the parent jets, are also different in the signal region and the control region. Therefore, extrapolation from the control region parametrized with only the photon p_{T} and η does not provide a precise enough description on the kinematic distributions of the leptons in the signal region.

We use the p_{T} of the dilepton pair as a proxy of the jet recoil in order to correct this bias. The dilepton p_{T} distribution of the predicted background events, obtained by applying the misidentification rate, is reweighted to match the correct shape of the dilepton p_{T} distribution of jet backgrounds in the signal region. The reweighting is done for separate photon p_{T} ranges in order to retain the yield and the photon p_{T} spectrum obtained from the previous step. After the correction, the lepton kinematic distributions from the total background prediction including the corrected data-driven background are in good agreement with the distributions in data.

6 Signal modeling

The production of an excited lepton involves one extra SM lepton, and therefore there are two possible pairings of a lepton with the photon. The corresponding two invariant masses are referred to as $M_{\ell\gamma}^{\mathrm{min}}$ and $M_{\ell\gamma}^{\mathrm{max}}$ in ascending order. The $M_{\ell\gamma}^{\mathrm{min}}$ and $M_{\ell\gamma}^{\mathrm{max}}$ distributions of observed data events and background estimates in the signal region are shown in Fig. 1.

A search window is set in the two dimensional distribution of $M_{\ell\gamma}^{\mathrm{min}}$ versus $M_{\ell\gamma}^{\mathrm{max}}$. For ℓ^* events, either $M_{\ell\gamma}^{\mathrm{min}}$ or $M_{\ell\gamma}^{\mathrm{max}}$ corresponds to the reconstructed invariant mass of ℓ^*. Therefore, the mass resonance of the signal is concentrated in the shape of a flipped "L" as shown in Fig. 2. On the other hand, background events have no such correlation in $M_{\ell\gamma}^{\mathrm{min}}$ and $M_{\ell\gamma}^{\mathrm{max}}$ and are scattered around at low masses $< 1\,\mathrm{TeV}$, as shown in Fig. 3. This clear distinction between signal and background events in the distribution of $M_{\ell\gamma}^{\mathrm{min}}$ versus $M_{\ell\gamma}^{\mathrm{max}}$ is used to define L-shaped search windows enhancing the discrimination between signal and background.

For low signal masses, $M_{\ell^*} \leq 1\,\mathrm{TeV}$, background suppression by setting an L-shaped search window outweighs the small loss in the signal acceptance. Therefore, the search window for $M_{\ell^*} \leq 1\,\mathrm{TeV}$ is set to be a narrow L-shape centered at M_{ℓ^*}, consisting of lower and upper thresholds of $M_{\ell\gamma}^{\mathrm{min}}$ and $M_{\ell\gamma}^{\mathrm{max}}$. For instance, for $M_{\mathrm{e}^*} = 500\,\mathrm{GeV}$, the search window is set to cover $\pm 8\%$ around the simulated mass, 460–540 GeV as shown in the left-hand plot of Fig. 2. The thresholds are optimized for the best expected exclusion limit with consideration for the impact of the energy scale and resolution uncertainties on the signal acceptance.

Search windows for $M_{\ell^*} > 1\,\mathrm{TeV}$, where the background contribution is expected to be negligible, are set wide by requiring only the lower $M_{\ell\gamma}^{\mathrm{max}}$ threshold, thereby maximizing the signal acceptance.

The product of signal acceptance and efficiency for excited electrons (muons) has been measured from the simulated signal samples, ranging from 30 (33)% to 48 (59)%, respectively. To determine the product of signal acceptance and efficiency for mass points other than those of the simulated samples, a polynomial fit to the dependence on M_{ℓ^*} is used for interpolation.

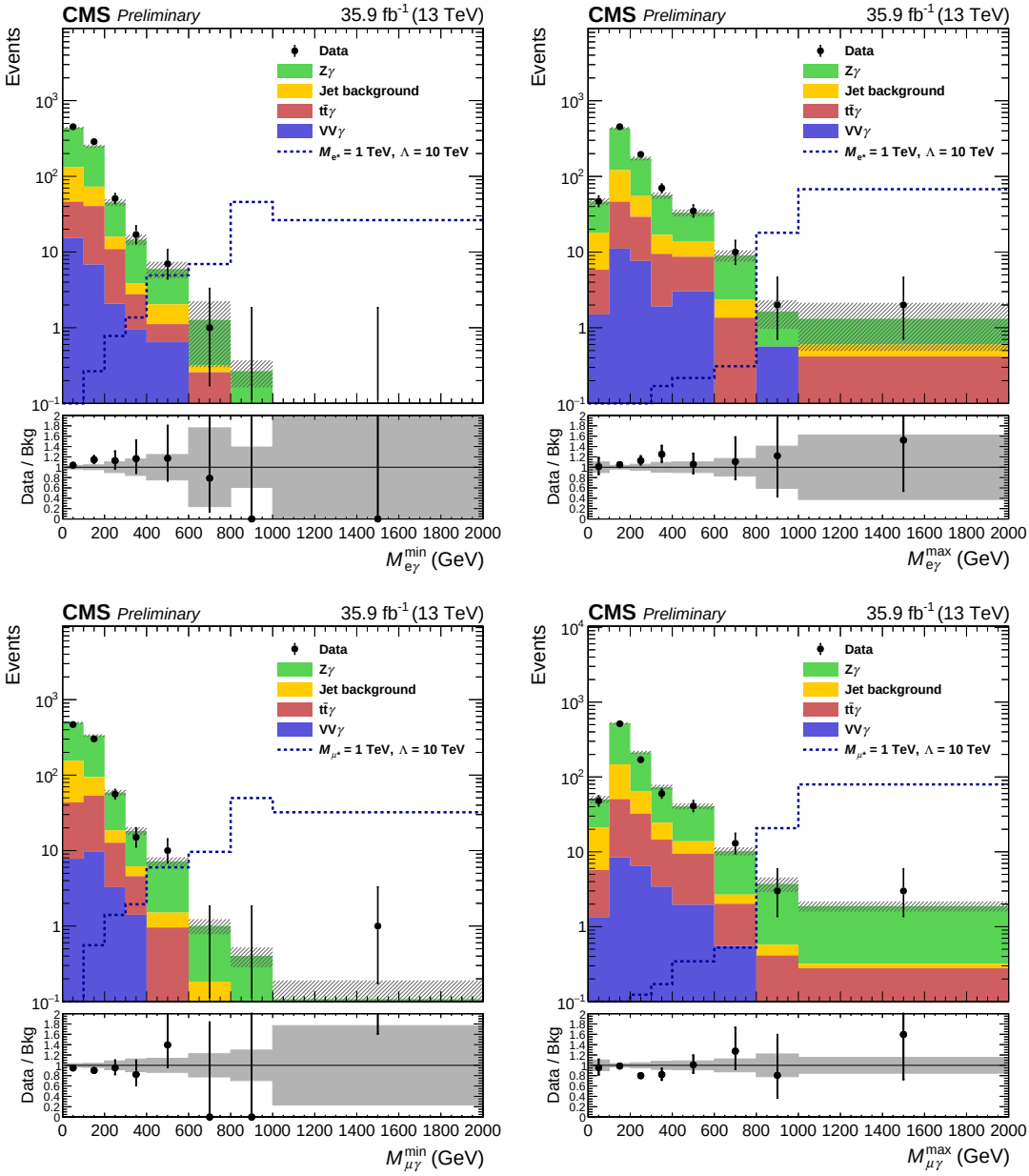

Figure 1: The distributions of $M_{\ell\gamma}^{\text{min}}$ (left panel) and $M_{\ell\gamma}^{\text{max}}$ (right panel) in the eeγ channel (upper panel) and the $\mu\mu\gamma$ channel (lower panel). The black dots denote the data points. The green, yellow, red and blue histograms correspond to the prediction of $Z\gamma$, the jet background, $\text{t}\bar{\text{t}}\gamma$, and triboson processes, respectively. The dotted lines represents ℓ^* signal events for $M_{\ell^*} = 1\,\text{TeV}$ at $\Lambda = 10\,\text{TeV}$.

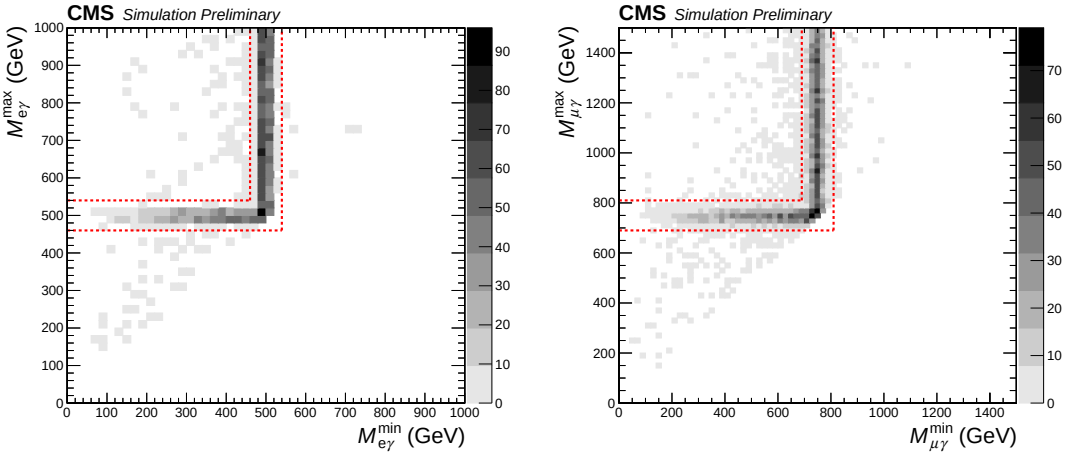

Figure 2: The two dimensional distributions of $M_{\ell\gamma}^{\text{min}}$ versus $M_{\ell\gamma}^{\text{max}}$ of excited electrons with a mass of 500 GeV (left) and of excited muons with a mass of 750 GeV (right), respectively, after event selection. The red dashed lines denote the boundary of the L-shaped search window for each mass point.

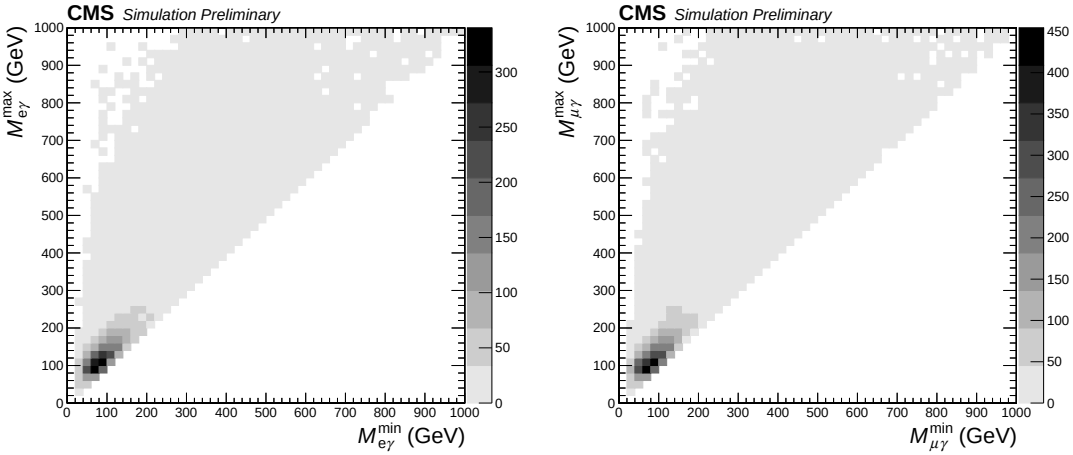

Figure 3: The two dimensional distributions of $M_{\ell\gamma}^{\text{min}}$ versus $M_{\ell\gamma}^{\text{max}}$ of $Z\gamma$ background events in the eeγ channel (left) and in the $\mu\mu\gamma$ channel (right), respectively, after event selection.

7 Systematic uncertainties

The systematic uncertainties in the signal and the background yields are summarized in Table 1. The statistical uncertainties in the data and the simulated samples used for background estimation are dominant in this search. Although the values of the systematic uncertainties in the data-driven methods appear large, their impact on the limits is small since the jet background makes up only 5–15% of the total background.

The luminosity has been measured with a precision of 2.5% [39], thus affecting the observed cross sections. The effect of pileup modeling on the selection efficiency is measured to be less than a percent over all mass points, and a conservative 1% uncertainty is assigned for it. Systematic uncertainties in the signal selection efficiency include uncertainties arising from trigger selection, and lepton and photon identification. Various sources of potential biases in the selection efficiency measurements are considered to determine such uncertainties. Uncertainties in the electron and photon energy scale and resolution and muon momentum scale and resolution translate to uncertainties in the signal acceptance. The effect on the signal acceptance is evaluated by shifting and smearing the p_{T} of each object by the corresponding uncertainty. The combined systematic uncertainty of the sources described above is approximately 5%.

Systematic uncertainties in the signal acceptance and background cross sections due to the PDF choice have been estimated by following the PDF4LHC prescription [40]. For QCD renormalization and factorization scale uncertainties, changes in the signal acceptance and the background cross sections due to various combinations of scale variations are determined, and the maximum observed change is assigned as an uncertainty. Uncertainties of 2 and 10% are assigned for the PDF and scale uncertainties in the signal acceptance and the background yields, respectively.

For the data-driven jet background estimation, the following uncertainties are taken into account: statistical uncertainties in the misidentification rate measurement, systematic uncertainties in the template distributions used for the fake rate measurement, and systematic uncertainties based on discrepancies observed from closure tests for the data-driven procedures. The total systematic uncertainty in the jet background prediction is evaluated by summing those uncertainties in quadrature, increasing to 90% for masses above 1 TeV.

Table 1: Summary of the systematic uncertainties (in %) in the signal yield, the prompt photon background prediction, and the jet background prediction.

Source	eeγ channel (%)			$\mu\mu\gamma$ channel (%)		
	Signal	Prompt γ bkg	Jet bkg	Signal	Prompt γ bkg	Jet bkg
Luminosity	2.5	2.5	-	2.5	2.5	-
Pileup	1	1	-	1	1	-
Trigger	1	1	-	2	2	-
Lepton efficiency	2.5	2.5	-	2	2	-
Photon efficiency	1.5	1.5	-	1.5	1.5	-
e/γ energy scale & resolution	2	2	-	2.5	2.5	-
μ momentum scale & resolution	-	-	-	2	2	-
PDF & scales	2	10	-	2	10	-
Data-driven bkg estimation	-	-	54–90	-	-	54–90
Statistical	-	8–44	5–47	-	10–25	6–58

8 Results

Within the uncertainties, the observed data are found to be consistent with the background prediction. We set the 95% confidence level (CL) upper limits on the production cross sec-

tions of excited electrons (e^*) and excited muons (μ^*), and the corresponding lower limits on the compositeness scale Λ, as a function of the excited lepton mass using a single-bin counting method [41]. The limits are computed with the modified frequentist CL_s method [42, 43], with a likelihood ratio used as a test statistic. The systematic uncertainties are treated as nuisance parameters with log-normal priors (normalization). The limits are set in the mass range between 0.25 and 5.0 TeV.

Figure 4 shows the 95% CL upper limits on the product of the signal cross section and branching fraction to the $\ell\ell\gamma$ final state, $\sigma \times \mathcal{B}(\ell\ell^* \to \ell\ell\gamma)$ (left panel), and lower limits on Λ (right panel), as a function of the resonance mass, for e^* (upper panel) and μ^* (lower panel). The observed limits are denoted by the solid black lines and the expected limits for the background-only hypothesis are represented by the dashed black lines. The 68 and 95% CL ranges are shown with the green and yellow bands, respectively.

The observed limits on the signal cross section ranges from 3 fb to 0.2 fb as a function of M_{ℓ^*} and are consistent with the expected limits. The gray, red, magenta, and blue dashed lines in the left-hand plots in Fig. 4 describe the theoretical cross sections including the NLO QCD correction factors for $\Lambda = M_{\ell^*}$, 10, 15, and 25 TeV, respectively.

A lower limit on M_{ℓ^*} depends on Λ since both M_{ℓ^*} and Λ are free parameters in the reference model. The observation excludes M_{ℓ^*} <3.9 (3.8) TeV for excited electrons (muons) in the case where $M_{\ell^*} = \Lambda$. The best observed limit on Λ is obtained in the mass range between 0.5 and 1.0 TeV, excluding Λ below 25 TeV for both excited electrons and muons. The representative limits are summarized in Table 2.

Table 2: Summary of the observed (expected) lower limits on M_{ℓ^*}, assuming $M_{\ell^*} = \Lambda$, and the best observed (expected) lower limits on Λ in the mass range 0.5–1.0 TeV.

Channel	Observed (expected) exclusion for $M_{\ell^*} = \Lambda$, TeV	Best observed (expected) limit on Λ, TeV
eeγ	3.9 (3.8)	25 (23)
$\mu\mu\gamma$	3.8 (3.9)	25 (23)

9 Summary

A search is presented for excited electrons and muons using a data sample of proton-proton collisions at a center-of-mass energy of $\sqrt{s} = 13$ TeV, collected with the CMS detector in 2016 and corresponding to an integrated luminosity of 35.9 fb^{-1}. This is the first search in the $\ell\ell\gamma$ final state in proton-proton collisions at $\sqrt{s} = 13$ TeV. The observed data are consistent with the standard model prediction, and exclusion limits on the excited lepton mass and the compositeness scale are set. Excited electrons (muons) with a mass below 3.9 (3.8) TeV are excluded under the assumption that the excited lepton mass equals the compositeness scale. The best observed limit on the compositeness scale is obtained in the mass range between 0.5 and 1.0 TeV, excluding a compositeness scale below 25 TeV for both excited electrons and muons. These are the most stringent limits to date in the $\ell\ell\gamma$ final state.

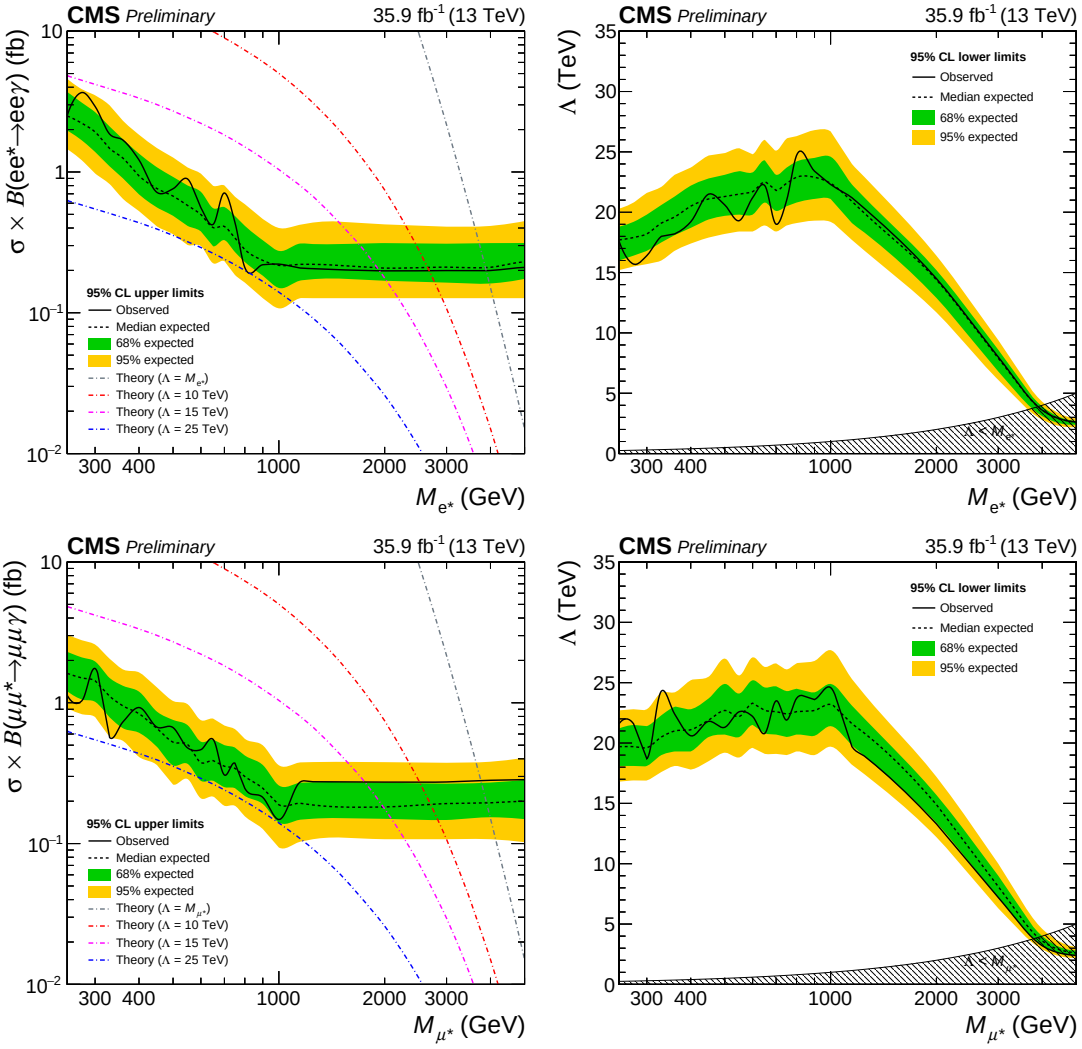

Figure 4: Observed (solid) and expected (dashed) 95% CL upper limits on the product of the production cross section and branching fraction (left panel) and lower limits on the compositeness scale (right panel) as a function of signal mass M_{ℓ^*}, together with the 68% (green) and 95% (yellow) CL ranges of the expected limit for the background-only hypothesis, for e* (upper panel) and μ^* (lower panel).

References

[1] J. C. Pati, A. Salam, and J. A. Strathdee, "Are quarks composite?", *Phys. Lett. B* **59** (1975) 265, doi:10.1016/0370-2693(75)90042-8.

[2] H. Terazawa, M. Yasuè, K. Akama, and M. Hayshi, "Observable effects of the possible substructure of leptons and quarks", *Phys. Lett. B* **112** (1982) 387, doi:10.1016/0370-2693(82)91075-9.

[3] M. Abolins et al., "Testing the Compositeness of Quarks and Leptons", in *Elementary Particles and Future Facilities (Snowmass 1982)*, p. 274. 1982. eConf C8206282.

[4] E. Eichten, K. D. Lane, and M. E. Peskin, "New Tests for Quark and Lepton Substructure", *Phys. Rev. Lett.* **50** (1983) 811, doi:10.1103/PhysRevLett.50.811.

[5] H. Harari, "Composite models for quarks and leptons", *Physics Reports* **104** (1984) 159, doi:10.1016/0370-1573(84)90207-2.

[6] K. D. Lane, F. E. Paige, T. Skwarnicki, and W. J. Womersley, "Simulations of supercollider physics", *Phys. Rept.* **278** (1997) 291, doi:10.1016/S0370-1573(96)00018-X, arXiv:hep-ph/9412280.

[7] U. Baur, M. Spira, and P. M. Zerwas, "Excited quark and lepton production at hadron colliders", *Phys. Rev. D* **42** (1990) 815, doi:10.1103/PhysRevD.42.815.

[8] O. W. Greenberg and C. A. Nelson, "Composite models of leptons", *Phys. Rev. D* **10** (1974) 2567, doi:10.1103/PhysRevD.10.2567.

[9] O. W. Greenberg and J. Sucher, "A quantum structure dynamic model of quarks, leptons, weak vector bosons, and Higgs mesons", *Phys. Lett. B* **99** (1981) 339, doi:10.1016/0370-2693(81)90113-1.

[10] S. Bhattacharya, S. S. Chauhan, B. C. Choudhary, and D. Choudhury, "Search for excited quarks in $q\bar{q} \to \gamma\gamma$ at the cern lhc", *Phys. Rev. D* **76** (2007) 115017, doi:10.1103/PhysRevD.76.115017.

[11] S. Bhattacharya, S. S. Chauhan, B. C. Choudhary, and D. Choudhury, "Quark Excitations Through the Prism of Direct Photon Plus Jet at the LHC", *Phys. Rev. D* **80** (2009) 015014, doi:10.1103/PhysRevD.80.015014, arXiv:0901.3927.

[12] CMS Collaboration, "Search for excited leptons in pp collisions at $\sqrt{s} = 7$ TeV", *Phys.Lett.* **B720** (2013) 309–329, doi:10.1016/j.physletb.2013.02.031, arXiv:1210.2422.

[13] CMS Collaboration, "Search for excited leptons in proton-proton collisions at $\sqrt{s} =$ 8 TeV", *JHEP* **03** (2016) 125, doi:10.1007, arXiv:1511.01407.

[14] ALEPH Collaboration, "Search for excited leptons at 130–140 GeV", *Phys. Lett. B* **385** (1996) 445, doi:10.1016/0370-2693(96)00961-6.

[15] DELPHI Collaboration, "Search for composite and exotic fermions at LEP 2", *Eur. Phys. J. C* **8** (1999) 41, doi:10.1007/s100529901074, arXiv:hep-ex/9811005.

[16] OPAL Collaboration, "Search for unstable heavy and excited leptons at LEP 2", *Eur. Phys. J. C* **14** (2000) 73, doi:10.1007/s100520050734, arXiv:hep-ex/0001056.

[17] L3 Collaboration, "Search for excited leptons at LEP", *Phys. Lett. B* **568** (2003) 23, doi:10.1016/j.physletb.2003.05.004, arXiv:hep-ex/0306016.

[18] H1 Collaboration, "Search for excited electrons in ep collisions at HERA", *Phys. Lett. B* **666** (2008) 131, doi:10.1016/j.physletb.2008.07.014, arXiv:0805.4530.

[19] CDF Collaboration, "Search for Excited and Exotic Electrons in the $e\gamma$ Decay Channel in $p\overline{p}$ Collisions at $\sqrt{s}$ = 1.96 TeV", *Phys. Rev. Lett.* **94** (2005) 101802, doi:10.1103/PhysRevLett.94.101802, arXiv:hep-ex/0410013.

[20] CDF Collaboration, "Search for Excited and Exotic Muons in the $\mu\gamma$ Decay Channel in $p\overline{p}$ Collisions at $\sqrt{s}$ = 1.96 TeV", *Phys. Rev. Lett.* **97** (2006) 191802, doi:10.1103/PhysRevLett.97.191802, arXiv:hep-ex/0606043.

[21] D0 Collaboration, "Search for excited muons in $p\overline{p}$ collisions at $\sqrt{s} = 1.96$ TeV", *Phys. Rev. D* **73** (2006) 111102, doi:10.1103/PhysRevD.73.111102, arXiv:hep-ex/0604040.

[22] D0 Collaboration, "Search for excited electrons in $p\overline{p}$ collisions at $\sqrt{s} = 1.96$ TeV", *Phys. Rev. D* **77** (2008) 091102, doi:10.1103/PhysRevD.77.091102, arXiv:0801.0877.

[23] ATLAS Collaboration, "Search for excited leptons in proton-proton collisions at $\sqrt{s}$ = 7 TeV with the ATLAS detector", *Phys. Rev. D* **85** (2012) 072003, doi:10.1103/PhysRevD.85.072003, arXiv:1201.3293.

[24] ATLAS Collaboration, "Search for excited electrons and muons in $\sqrt{s}$ = 8 TeV proton-proton collisions with the ATLAS detector", *New J. Phys.* **15** (2013) 093011, doi:10.1088/1367-2630/15/9/093011, arXiv:1308.1364.

[25] CMS Collaboration, "The CMS experiment at the CERN LHC", *JINST* **3** (2008) S08004, doi:10.1088/1748-0221/3/08/S08004.

[26] CMS Collaboration, "The CMS trigger system", *JINST* **12** (2017) P01020, doi:10.1088/1748-0221/12/01/P01020, arXiv:1609.02366.

[27] T. Sjostrand, S. Mrenna, and P. Skands, "A Brief Introduction to PYTHIA 8.1", *Comput. Phys. Commun.* **178** (2008) 852, doi:10.1016/j.cpc.2008.01.036, arXiv:0710.3820.

[28] P. Skands, S. Carrazza, and J. Rojo, "Tuning PYTHIA 8.1: the Monash 2013 tune", *Eur. Phys. J. C* **74** (2014) 3024, doi:10.1140/epjc/s10052-014-3024-y, arXiv:1404.5630.

[29] CMS Collaboration, "Event generator tunes obtained from underlying event and multiparton scattering measurements", *Eur. Phys. J. C* **76** (2016) 155, doi:10.1140/epjc/s10052-016-3988-x, arXiv:1512.00815.

[30] S. Majhi, "QCD corrections to excited lepton (pair) production at the LHC", *Phys. Rev. D* **88** (2013), no. 7, 074028, doi:10.1103/PhysRevD.88.074028, arXiv:1210.8307.

[31] J. Alwall et al., "The automated computation of tree-level and next-to-leading order differential cross sections, and their matching to parton shower simulations", *JHEP* **07** (2014) 079, doi:10.1007/JHEP07(2014)079, arXiv:1405.0301.

[32] CMS Collaboration, "Particle-flow reconstruction and global event description with the cms detector", *JINST* **12** (2017) P10003, doi:10.1088/1748-0221/12/10/P10003, arXiv:1706.04965.

[33] M. Cacciari, G. P. Salam, and G. Soyez, "The anti-k_t jet clustering algorithm", *JHEP* **04** (2008) 063, doi:10.1088/1126-6708/2008/04/063, arXiv:0802.1189.

[34] M. Cacciari, G. P. Salam, and G. Soyez, "FastJet user manual", *Eur. Phys. J. C* **72** (2012) 1896, doi:10.1140/epjc/s10052-012-1896-2, arXiv:1111.6097.

[35] CMS Collaboration, "Performance of the CMS muon detector and muon reconstruction with proton-proton collisions at $\sqrt{s}$ = 13 TeV", (2018). arXiv:1804.04528. Submitted to JINST.

[36] CMS Collaboration, "Electron and Photon performance using data collected by CMS at $\sqrt{s}$ = 13 TeV and 25ns", *CMS Detector Performance Summary CMS-DP-2015-067* (2015).

[37] CMS Collaboration, "Performance of Photon Reconstruction and Identification with the CMS Detector in Proton-Proton Collisions at $\sqrt{s}$ = 8 TeV", *JINST* **10** (2015), no. 08, P08010, doi:10.1088/1748-0221/10/08/P08010, arXiv:1502.02702.

[38] CMS Collaboration, "Search for high-mass resonances in dilepton final states in proton-proton collisions at $\sqrt{s}$ = 13 TeV", *JHEP* **06** (2018) 120, doi:10.1007/JHEP06(2018)120, arXiv:1803.06292.

[39] CMS Collaboration, "CMS luminosity measurements for the 2016 data-taking period", CMS Physics Analysis Summary CMS-PAS-LUM-17-001, 2017.

[40] J. Butterworth et al., "PDF4LHC recommendations for LHC Run II", *J. Phys. G* **43** (2016) 023001, doi:10.1088/0954-3899/43/2/023001, arXiv:1510.03865.

[41] ATLAS and CMS Collaborations, "Procedure for the LHC higgs boson search combination in Summer 2011", Technical Report CMS-NOTE-2011-005, ATL-PHYS-PUB-2011-011, CERN, Geneva, 2011.

[42] T. Junk, "Confidence level computation for combining searches with small statistics", *Nucl. Instrum. Meth. A* **434** (1999) 435, doi:10.1016/S0168-9002(99)00498-2, arXiv:hep-ex/9902006.

[43] A. L. Read, "Presentation of search results: the CL_s technique", *J. Phys. G* **28** (2002), no. 10, 2693, doi:10.1088/0954-3899/28/10/313.